

# PRECISE FREQUENCY TUNING OF S-BAND PULSE COMPRESSORS AT HIGH-POWER OPERATION IN THE ELECTRON AND POSITRON INJECTOR LINAC OF KEK

H. Ego<sup>†,1</sup>, S. Ushimoto<sup>2</sup>

<sup>1</sup>KEK, Ibaraki, Tsukuba, Japan

<sup>2</sup>Mitsubishi Electric System & Service Co., Ltd, Ibaraki, Tsukuba, Japan

## Abstract

The KEK electron-positron injector linac employs pulse compressors to amplify high-power radio frequency waves generated by S-band 40-MW klystrons. Accurate tuning of these compressors during high-power operation is essential to minimize their voltage standing wave ratio and maximize output power. We developed a real-time, labor-saving tuning system that consists of a waveform analyzer and a removable remote-controlled tuner driver. The analyzer calculates frequency deviations and waveform distortions in real-time by comparing the compressor’s output waveform to an optimal waveform derived from fourth-order Runge–Kutta calculations. The tuner eliminates frequency deviations, whereas the analyzer monitors pulse-to-pulse adjustments. Consequently, all compressors were tuned efficiently and precisely.

## INTRODUCTION

The KEK electron-positron injector linac currently operates 60 S-band, i.e., 2856 MHz, acceleration units at a frequency of 50 Hz. Figure 1 illustrates the typical configuration of the unit where the radio frequency (RF) output from the klystron is compressed and amplified by a pulse compressor before being fed into four accelerating structures. SLAC energy doublers (SLEDs) [1] serve as pulse compressors and are installed in 56 units. Figure 2 shows a photo of the SLED. It consists of a 3-dB hybrid coupler and two cylindrical high- $Q$  cavities; its RF properties are listed in Table 1. From 2022, single-cavity pulse compressors were introduced to replace SLEDs and are currently in stable operation [2].

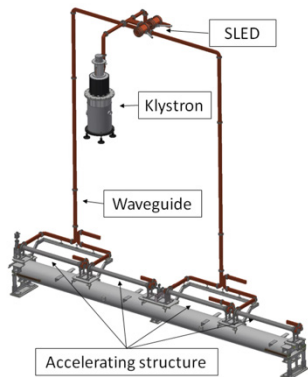


Figure 1: S-band acceleration unit

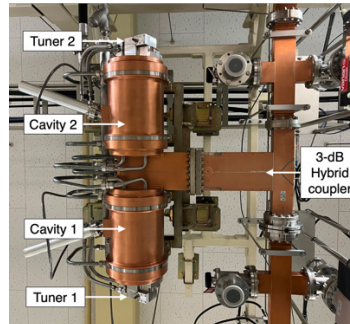


Figure 2: SLED in the KEK injector linac

This study presents improvements to the SLED tuning method and the latest results. Tuning the cavities to the operating frequency during rated high-power operation is necessary to ensure the SLED achieves optimal output. Conventional tuning methods have involved measuring RF waveforms with an oscilloscope and manually adjusting tuners attached to the cavities, relying heavily on the operator’s visual judgment to maximize peak output and minimize reflections. This approach was unclear about whether the SLED was accurately tuned to the operating frequency. To address this, we developed a waveform analyzer and a removable remote tuning controller to enable easy and precise tuning of the SLED at the operating frequency.

Table 1: SLED’s RF Characteristics

Operating frequency [MHz]	2,856
Resonant mode	TE <sub>015</sub>
Unloaded $Q$ ( $Q_0$ )	100,000
Coupling coefficient $\beta$	6.4
Peak voltage compression ratio	6.2
Input pulse length [ $\mu$ s]	4.0
Phase-reversed duration [ $\mu$ s]	1.0
Input power [MW]	40

## PRECISE TUNING TOOLS

### Waveform Analyzer

The control system was significantly improved as part of the injector upgrade to facilitate simultaneous top-up injection into the downstream storage rings [3]. A new precise timing system enabled synchronization of all pulse-driven accelerator components at 50 Hz [4]. Synchronous RF waveform monitors were introduced, and

<sup>†</sup> ego@post.kek.jp

were remotely accessible via an EPICS-based control system [5].

The waveform analyzer, programmed in Windows LabVIEW [6], captured SLED waveforms from RF monitors instead of oscilloscopes, analyzed them, and estimated the SLED's resonant frequency in real-time. Figure 3 displays a screenshot of the analyzer in use. The analyzer shows current waveforms on the left and the tuning progress and klystron status on the right. The displayed data include:

- (a) Amplitudes of the measured waveform (white line) and optimal waveform (red line).
- (b) Amplitude deviation between the measured and optimal waveforms.
- (c) Phases of the measured (white) and optimal (red) waveforms.
- (d) Time chart of the integral value of amplitude deviations.
- (e) History of the resonant frequency.
- (f) Klystron operating status.

The optimal waveform is derived from the incident waveform by numerically solving the following differential equations for the SLED using the fourth-order Runge–Kutta method:

$$\left(1 + \frac{\omega_{c,1}^2}{\omega^2}\right) \frac{dV_{c,1}}{dt} + \left\{ \frac{\omega_{c,1}}{Q_{L,1}} + j\omega \left(1 - \frac{\omega_{c,1}^2}{\omega^2}\right) \right\} V_{c,1} = \frac{2\omega_{c,1}\beta_1}{Q_{0,1}} \frac{V_i}{\sqrt{2}}, \quad (1)$$

$$\left(1 + \frac{\omega_{c,2}^2}{\omega^2}\right) \frac{dV_{c,2}}{dt} + \left\{ \frac{\omega_{c,2}}{Q_{L,2}} + j\omega \left(1 - \frac{\omega_{c,2}^2}{\omega^2}\right) \right\} V_{c,2} = \frac{2\omega_{c,2}\beta_2}{Q_{0,2}} \frac{jV_i}{\sqrt{2}}, \quad (2)$$

and

$$V_o = \frac{1}{\sqrt{2}} (jV_{c,1} + V_{c,2}), \quad (3)$$

where  $\omega$  is the operating angular frequency,  $V_i$  is the voltage of the incident wave,  $V_o$  is the output voltage,  $\omega_{c,1}$ ,  $Q_{L,1}$ ,  $Q_{0,1}$ , and  $\beta_1$  are the resonant angular frequency, loaded  $Q$ , unloaded  $Q$ , and coupling coefficient of one of the cavities, respectively, and  $\omega_{c,2}$ ,  $Q_{L,2}$ ,  $Q_{0,2}$ , and  $\beta_2$  are the resonant angular frequency, loaded  $Q$ , unloaded  $Q$ , and coupling coefficient of the other cavities, respectively. Equations (1) and (2) describe the cavities' responses to the incident wave and Equation (3) shows that  $V_o$  results from the superposition of the outputs of the two cavities via the 3-dB hybrid.

During tuning, the klystron modulator charging voltage ( $E_s$ ), klystron output power ( $P_f$ ), reflection power ( $P_b$ ), and voltage standing wave ratio (VSWR) were monitored to prevent unnecessary interlocks triggered by a sudden increase in  $P_b$ . The SLED resonant frequency was estimated from the integral of amplitude deviation. These processes occurred in real-time and pulse-to-pulse at 50 Hz, allowing for precise estimation regardless of fluctuations in the incident wave.

The tuning objective was to minimize the integral of amplitude deviation. The measured waveform was adjust-

ed by the remote-controlled tuner to align with the optimal waveform, thereby reducing  $P_b$ .

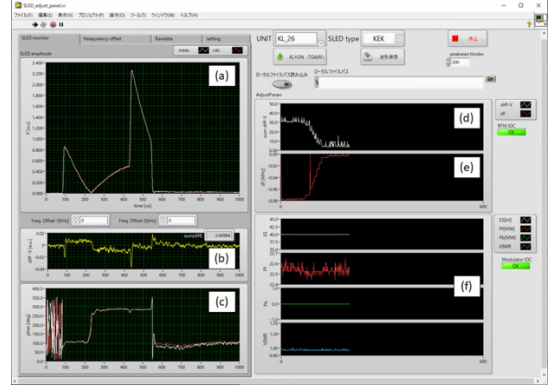


Figure 3: Waveform analyzer

### Remote Tuning Mechanics

Each of the SLED cavities is equipped with a manual worm wheel tuner, which can adjust the cavity resonant frequency at a rate of 4.4 kHz/mm. We developed a remote controller for wheel adjustment that consists of a removable stepping-motor unit and a motor driver. The driver includes a microcomputer (Arduino Mega2560 [7]) that handles control buttons on the front panel, two stepping-motor driving modules (Strawberry Linux DRV8825 [8]), and DC power supplies. These modules were operated in 1/16 micro-stepping mode. Figure 4 shows the remote controller and the tuner with the stepping-motor unit. By attaching the stepping-motor units to the tuners and utilizing this controller, cavity resonant frequencies were precisely adjusted in 0.055-kHz steps, a feat that is unachievable with manual control.

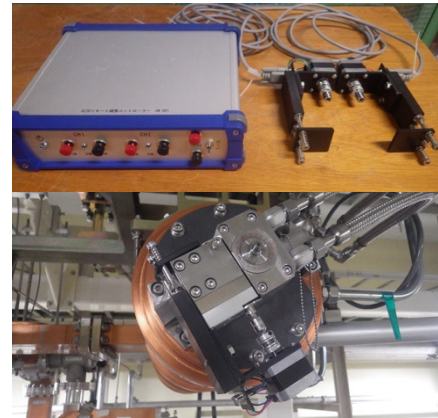


Figure 4: Remote controller (upper) and tuner mounted with the stepping-motor unit (lower)

## TUNING RESULTS

Figure 5 illustrates the changes in the SLED output waveform resulting from tuning. The blue and orange solid lines represent the waveform before and after tuning, respectively, whereas the green line denotes the estimated optimal waveform. Following tuning, the amplitude dip occurring at approximately 1.7  $\mu$ s was reduced to

approximately zero, aligning with the optimal waveform, confirming that both cavities were tuned to the operating frequency. The unnecessary tail in amplitude observed after 4.5  $\mu\text{s}$  was eliminated, and the measured waveform closely matched the estimated waveform. The phase also approached the optimal values. The phase step noted at the rapid amplitude increase of 3.5  $\mu\text{s}$  was removed, as the SLED frequency was tuned to the operating frequency. This confirmed that the SLED output almost perfectly reproduced the optimal waveform.

Using the new tuning system, a single operator performed the measurement and tuning work in approximately 10 to 15 min per SLED. This represents a notable reduction in manpower and time compared to conventional methods that involve oscilloscopes and require four operators.

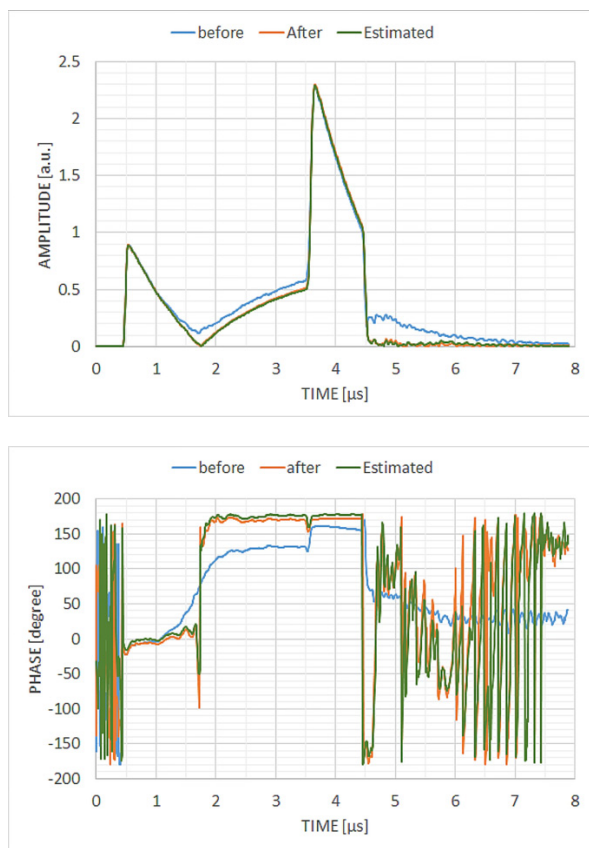


Figure 5: Amplitude (upper) and phase (lower) of the waveforms before (blue lines) and after (orange lines) tuning. Each green line shows the estimated optimal waveform.

## SUMMARY

To address the limitations of previous SLED tuning methods, we developed a waveform analyzer and implemented remote-controlled tuners for the SLED cavities. This innovation has led to a notable reduction in tuning time compared to conventional methods and confirmed that optimal SLED tuning can be readily achieved.

## ACKNOWLEDGEMENTS

The authors would like to extend their gratitude to the staff of the accelerating structure and positron source R&D group for useful discussions and the linac operators of Mitsubishi Electric System & Service Co., Ltd. for their support.

## REFERENCES

- [1] Z. D. Farkas *et al.*, “SLED: A Method of Doubling SLAC’s Energy”, in *Proc. Of 9th Int. Conf. On High Energy Accelerators*, SLAC, Stanford, California, 1974, pp. 576-583.
- [2] H. Ego *et al.*, “Upgrades of S-band Accelerating Structures and Pulse Compressors in the Electron and Positron Injector Linac of KEK”, in *Proc. IPAC’23*, Venice, Italy, May 2023, pp. 2932-2935.  
[doi:10.18429/JACoW-IPAC2023-WEPA118](https://doi.org/10.18429/JACoW-IPAC2023-WEPA118)
- [3] M.Satoh *et al.*, “The KEK Injector Upgrade for the Fast Beam-Mode Switch”, in *Proc. the 31st Linear Accelerator Meeting in Japan*, Sendai, August 2006, pp. 499-501.
- [4] T. Kudou *et al.*, “The Event Timing System in KEK Linac”, in *Proc. PASJ2010*, Himeji, Japan, August 2010, pp. 653-655.
- [5] H Katagiri *et al.*, “RF Monitor Unit for Simultaneous Injection”, in *Proc. PASJ2012*, Osaka, August 2012, pp. 753-756.
- [6] <https://www.ni.com/>
- [7] ArduinoStore, “Arduino Mega 2560 Rev3”, <https://store.arduino.cc/products/arduino-mega-2560-rev3>
- [8] Strawberry Linux, “DRV8825”, <https://strawberry-linux.com/catalog/items?code=12025>